Control of a Zero-Voltage Switching Isolated Series-Resonant Power Circuit for Direct 3-phase AC to DC Conversion

Yusuf Kosesoy, Remco Bonten, Henk Huisman, Jan Schellekens
Eindhoven University of Technology
Eindhoven, The Netherlands
y.k.kosesoy@tue.nl

Acknowledgement

This project has received funding from the ECSEL Joint Undertaking (JU) under grant agreement No 101007281. The JU receives support from the European Union's Horizon 2020 research and innovation programme and Austria, Germany, Slovenia, Netherlands, Belgium, Slovakia, France, Italy, Turkey.

Keywords

≪Soft Switching≫, ≪ZVS Converter≫, ≪Resonant Converter Control≫, ≪Fast Transient Response≫.

Abstract

A novel control method is presented for a fully zero-voltage switching series-resonant isolated 3-phase AC to DC converter. The control is derived from first principles such as energy and charge conservation. The approach results in operation with a high power factor at the AC grid side and is beneficial in terms of EMI due to soft switching and low dv/dt across the switches even when extremely fast WBG devices such as SiC or GaN are used.

Introduction

The application of the newest generation of Wide-Bandgap (WBG) devices in classical, hard-switching power circuits leads to extremely steep voltages at the switching nodes and as a consequence to large amounts of electromagnetic interference (EMI). With such circuits, switching times in the order of a few nanoseconds are observed [1], and voltage slopes up to several tens and even above one hundred volts per ns [2]. These very steep slopes give rise to a large amount of both differential and common-mode EMI. Typically, EMI in power converters is attenuated by means of filters, which represent between 20-40% of the volume and weight of the total assembly [3]. With the steep slopes caused by hard-switching WBG devices, the design of such filters becomes increasingly difficult, as parasitic elements in the filter components become more relevant. Due to the presence of inter-winding capacitance in inductors and parasitic series inductance in capacitors, a filter which was designed to show low-pass behaviour actually becomes high-pass at the frequencies related to the very fast switching, thereby losing (part of) its function.

It can be expected that due to the developments described above, the relative volume, weight and cost of EMI filters will have to increase, which is not a very attractive outlook: the gain in efficiency and size of the core power processor due to using WBG devices is at least partially lost due to increased filter size and losses. Therefore, in this paper, we will present an approach which attempts to avoid hard-switching and thereby eliminate the root cause for the high-frequency EMI. Similar approaches (ZVS) have already been shown for some classes of DC-DC converters such as full/half bridge driven resonant circuits [4]-[6], DAB circuits [8, 7] and SR circuits [9]. The approach will be illustrated by means of a direct three-phase AC to DC converter. The circuit of this converter was proposed in [10], but a suitable control law to facilitate soft switching and experimental results are still missing.

Circuit operation

The proposed circuit is shown in Figure 1. It consists of a 4-phase voltage selector using 8 MOSFET devices (Q1..Q8) which are pair-wise connected in anti-series, a resonant tank (C_{res},L_{res}), an isolation transformer also for scaling and a diode rectifier bridge supplying the load. The AC supply is represented as three ideal voltage sources ($V_R \cdots V_T$) combined with the neutral ($V_Z = 0$). In the sequel we will assume the AC supply to be balanced, in particular that the sum of the AC voltages is zero.

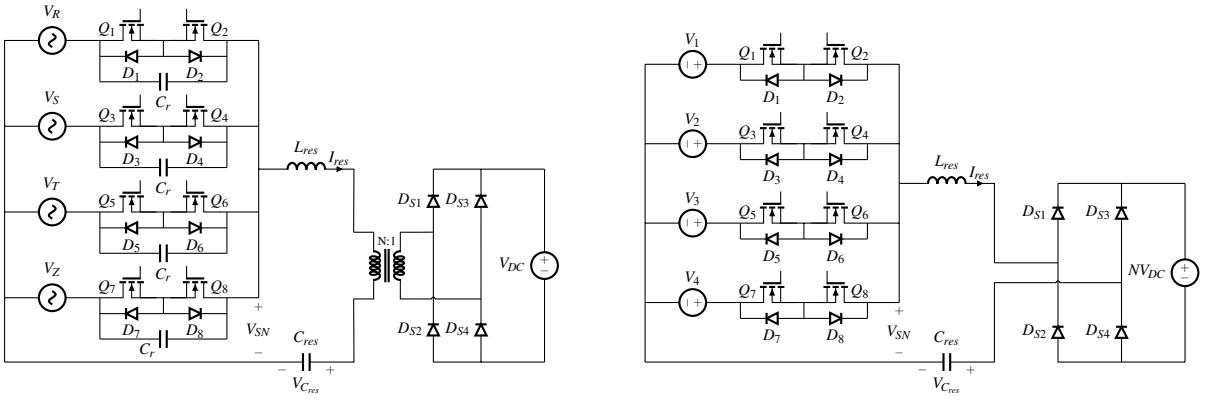

(a) (b)

Fig. 1: Direct three-phase to DC converter (a) proposed circuit; (b) simplified circuit for control method.

We will address the operation of the circuit as shown in Figure 1a during one cycle of the resonant tank, i.e. from one rising zero crossing of the resonant current I_{res} to the next. To simplify the analysis, we will assume that the voltages both at the supply and load sides are constant for the duration of the resonant cycle, and can therefore be represented by DC sources. Also, the transformer, which is assumed to be ideal and has turns ratio N, is removed with a corresponding change in naming for the DC source representing the load ($V_{DC} \rightarrow NV_{DC}$). The effect of the device capacitances is represented by capacitances C_r. Note that it is possible to place extra capacitance here to further reduce the value of dV/dt. However, the influence of these capacitances and losses in the circuit are ignored for the analysis in this research.

The voltages at the supply side (including the neutral voltage) will be sorted from most positive to most negative, and receive a numerical subscript for the analysis to follow. Once these simplifications/modifications have been implemented, the circuit can be depicted as shown in Figure 1b. Due to the sorting of the voltages, V_1 and V_2 will always be non-negative, and V_3 and V_4 non-positive.

To obtain zero voltage switching (ZVS) in the half-cycle where $I_{res} > 0$, the generalized supply voltages need to be applied starting with the most positive (i.e. V_1) and ending with the most negative (V_4). For the other half-cycle, where $I_{res} < 0$, the inverse applies: this half-cycle needs to start at V_4 and end at V_1. The behaviour over a complete resonant cycle can be depicted as shown in Figure 2.

As shown in Figure 2a, the complete resonant cycle is composed of 8 sub-intervals. During each of these, one of the AC side voltages $V_1 \cdots V_4$ is applied to the left of the resonant tank which represents V_{SN}. The interval boundaries are defined by the switching on/off of the MOSFETs at the AC side and the diodes at the load side.

In the switching modulation, at the rising zero crossing of resonant current, the MOSFETs Q1, Q3, Q5 and Q7 are turned on under zero current switching (ZCS) conditions, but only the phase with the highest voltage, phase V_1, provides energy to the resonant circuit through the diode D_2 while the diodes D_4, D_6 and D_8 are blocking and prevent any short circuit between the phases. Afterwards, the MOSFET in parallel the conducting diode, Q_2, can be turned on under ZVS conditions. The amount of charge to be delivered from each phase for one full resonant cycle is calculated using the energy balance approach at the beginning of the cycle. When the calculated amount of charge for the phase V_1 is provided, the MOSFET Q_1 is turned off. The second highest phase, phase V_2, can provide energy over the MOSFET Q_3 only after the V_{SN} voltage drops to the voltage level of V_2, through the D_4 diode and the ZVS conditions

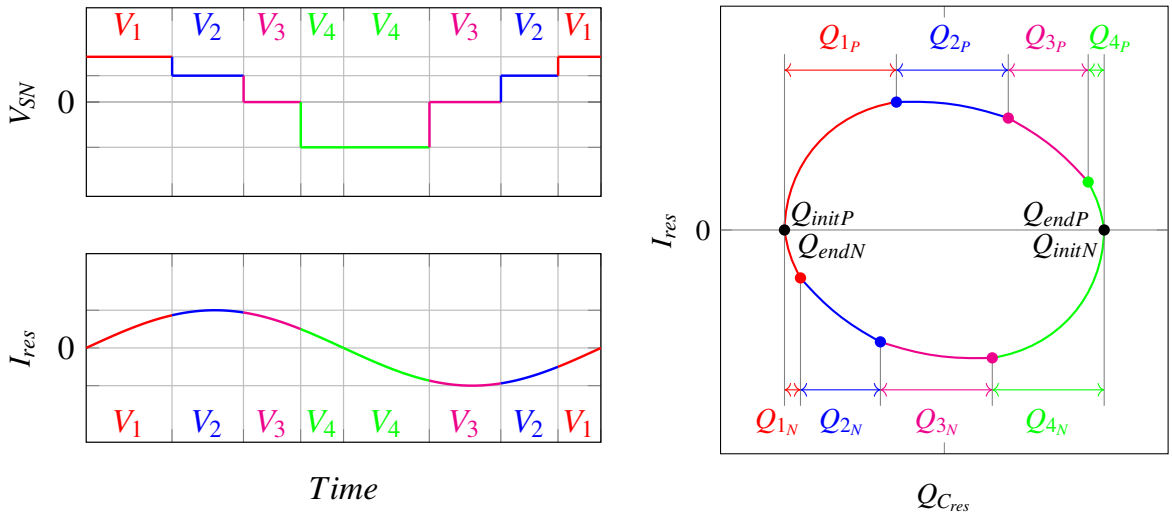

(a) (b)

Fig. 2: Example of waveforms for two positive and one negative phase voltages (a) applied voltage to the resonant tank and resonant current, (b) state-plane diagram.

are satisfied for the Q_4 MOSFET to be turned on. In this simplified model, the change on V_{SN} occurs instantaneously as the node capacitance, C_r, is ignored. This procedure continues for all the phase transitions in the positive half cycle. A similar procedure applies for the negative half-cycle. Consequently, soft switching is achieved throughout the circuit operation.

The operation of the circuit is also depicted in Figure 2b in the state plane spanned by the resonant charge $Q_{C_{res}}$ (i.e. the charge stored in C_{res}) and the resonant current I_{res} by using the approach presented in [11]. Note that when resonant capacitor C_{res} is linear, a representation using the voltage V_{Cres} across it would look exactly the same, apart from the obvious scaling with value C_{res}. However, a description using charges leads to somewhat simpler expressions, and is also applicable for the case when C_{res} shows non-linear behaviour, as would be the case for some varieties of ceramic capacitors.

The frequency of the inductor current, to be pointed out, is slightly higher than the resonant frequency, but it is not a control parameter, but a consequence of the control technique. The excess frequency of the inductor current can be observed on the state plane from the inflection at each phase transition. Also, the frequency of the inductor current increases as the load decreases which could be possible to observe in the state plane since there is going to be more inflection for light loads.

Some important variables, to be used in the derivation which follows, are shown there: the initial charge on C_{res} for the positive half-cycle is depicted as Q_{initP}, similar for the end of the half-cycle and for the negative half-cycle. As we consider a single cycle starting at a positive zero crossing for I_{res}, we find $Q_{initN} = Q_{endP}$. However, it is not necessarily the case that $Q_{initP} = Q_{endN}$, this holds only when steady-state operation is assumed.

The charges provided or absorbed by the AC supply per sub-interval have been depicted as $Q_{1P} \cdots Q_{4N}$. For the positive and negative half-cycles respectively we find the following relations:

$$\begin{aligned} Q_{DC_P} &= Q_{endP} - Q_{initP} = Q_{1P} + Q_{2P} + Q_{3P} + Q_{4P}, \\ Q_{DC_N} &= Q_{endN} - Q_{initN} = Q_{4N} + Q_{3N} + Q_{2N} + Q_{1N}. \end{aligned} \tag{1}$$

Note that all charges with subscript ..N are negative. Due to the diode rectifier at the load side, these are also the net charges per interval which flow (after rectification) to the load.

The energy balances for the positive and negative half-cycles can respectively be formulated as:

$$
\begin{aligned}
Q_{1P}V_1 + Q_{2P}V_2 + Q_{3P}V_3 + Q_{4P}V_4 - Q_{DC_P}NV_{DC} &= \frac{Q_{endP}^2 - Q_{initP}^2}{2C_{res}}, \\
Q_{1N}V_1 + Q_{2N}V_2 + Q_{3N}V_3 + Q_{4N}V_4 + Q_{DC_N}NV_{DC} &= \frac{Q_{endN}^2 - Q_{initN}^2}{2C_{res}}.
\end{aligned} \tag{2}
$$

The net charge per full resonance cycle supplied by phase V_1 equals $Q_1 = Q_{1P} + Q_{1N}$, and similar for the other phases. By adding the two parts of (2), the energy balance for the full cycle can be expressed as:

$$
Q_1V_1 + Q_2V_2 + Q_3V_3 + Q_4V_4 + (Q_{DC_N} - Q_{DC_P})NV_{DC} = \frac{Q_{endP}^2 - Q_{initP}^2 + Q_{endN}^2 - Q_{initN}^2}{2C_{res}}. \tag{3}
$$

Steady state

Under steady state conditions ($Q_{initP} = Q_{endN}$ and $Q_{initN} = Q_{endP}$), the right-hand side of (3) vanishes, and using (1), (3) can be further simplified to:

$$
Q_1V_1 + Q_2V_2 + Q_3V_3 + Q_4V_4 = 2Q_{DC}NV_{DC} \tag{4}
$$

where due to the steady state we can use $Q_{DC} = Q_{DC_P} = -Q_{DC_N}$. Note that either V_2 or V_3 is always zero and the corresponding (neutral) phase is only conducting current until the net charge reaches its final value after the active phases. To obtain a maximum power factor, the net charge per phase is chosen linearly proportional to the supply voltage as:

$$
Q_1 = KV_1, Q_2 = KV_2, Q_3 = KV_3, Q_4 = KV_4 \tag{5}
$$

in which K is a constant with the dimension of capacitance. Applying this to the energy balance (4), we obtain:

$$
KV_1^2 + KV_2^2 + KV_3^2 + KV_4^2 = 2Q_{DC}NV_{DC} \rightarrow K = \frac{2Q_{DC}NV_{DC}}{V_1^2 + V_2^2 + V_3^2 + V_4^2} \tag{6}
$$

To avoid the flow of reactive current, combinations of charge and voltage which lead to negative power flow will be discarded. For this purpose it is now suitable to distinguish two cases:

Case 1 (12Z4 sequence)
The case relates to the situation where two of the AC supply voltages are positive and the remaining one negative. In this case it follows that $V_1 > 0, V_2 > 0, V_3 = 0, V_4 < 0$. Hence, as $Q_{4P} > 0$, the interval related to V_4 can be discarded/skipped for the positive resonant half-cycle, and similarly V_1 and V_2 can be skipped for the negative half-cycle. In other words this implies that $Q_{1N} = 0$, $Q_{2N} = 0$, $Q_{4P} = 0$.

Case 2 (1Z34 sequence)
The other case applies to the opposite situation: one supply voltage is positive and the two others negative. In this case we find $V_1 > 0, V_2 = 0, V_3 < 0, V_4 < 0$. Here, both V_3 and V_4 can be skipped for the positive half-cycle, and V_1 for the negative half-cycle. This implies that $Q_{1N} = 0$, $Q_{3P} = 0$, $Q_{4P} = 0$. As a result, the general state plane diagram as depicted in Figure 2b changes to the two varieties depicted in Figure 3.

In order to simplify the expressions, the average charge, Q_{AV}, is defined as in (7).

$$
Q_{AV} = (Q_{endP} + Q_{initP})/2 \tag{7}
$$

Using (6) and (7), (2) can be rewritten for case 1 as in (8):

$$
\begin{aligned}
(V_1^2 + V_2^2)\frac{2Q_{DC}NV_{DC}}{V_1^2 + V_2^2 + V_3^2 + V_4^2} - Q_{DC}NV_{DC} &= \frac{Q_{DC}Q_{AV}}{C_{res}}, \\
(V_3^2 + V_4^2)\frac{2Q_{DC}NV_{DC}}{V_1^2 + V_2^2 + V_3^2 + V_4^2} - Q_{DC}NV_{DC} &= -\frac{Q_{DC}Q_{AV}}{C_{res}}.
\end{aligned} \tag{8}
$$

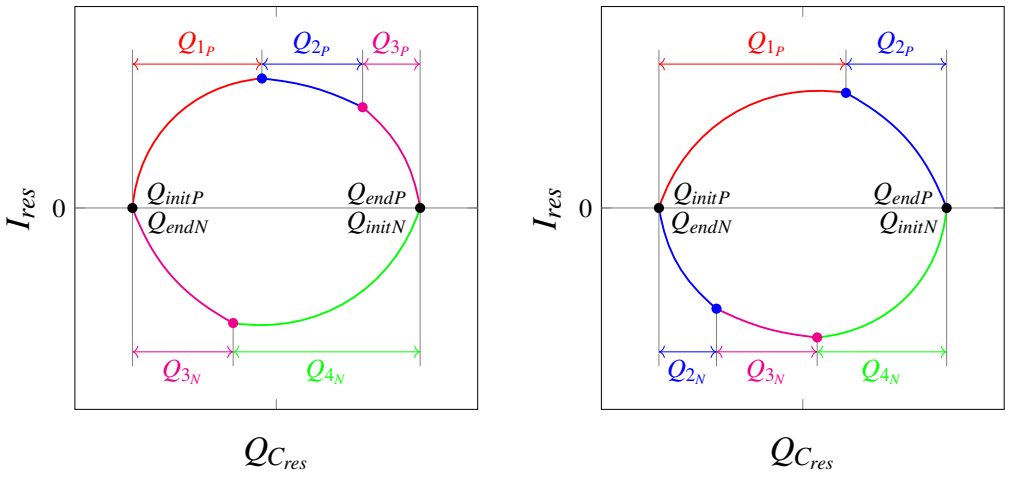

Fig. 3: Example of state-plane diagrams, (a) case 1 and (b) case 2.

For case 2 exactly the same result is found. After some manipulation of (8) we find for the average charge Q_{AV}:

$$Q_{AV} = \frac{V_1^2+V_2^2-V_3^2-V_4^2}{V_1^2+V_2^2+V_3^2+V_4^2} NV_{DC}C_{res}. \tag{9}$$

Note that (9) holds for both case 1 and 2, and that Q_{AV} will be continuous at the transitions between these cases. Furthermore, (9) implies that the state plane trajectory will in general not be centered around (0,0), as would be the usual case for most resonant converters.

Transient operation

In this section we will derive equations for the transient operation, in which Q_{endN} is not necessarily equal to Q_{initP}. As a first step, the energy balances per half cycle in (2) are re-used. Just as for the steady-state derivation, we will assume that the charge displacements are made linearly proportional to the applied AC-side voltage. Also here, intervals which lead to negative power flow at the AC side will be discarded. Hence we find the charge displacements for the case 1 and case 2, respectively:

$$\begin{aligned} &Q_{1P} = K_P V_1, Q_{2P} = K_P V_2, Q_{4N} = K_N V_4, \\ &Q_{1P} = K_P V_1, Q_{3N} = K_N V_3, Q_{4N} = K_N V_4. \end{aligned} \tag{10}$$

with K_P, K_N again proportionality constants with the dimension of capacitance. Using these constants, (2), leaving out the undesired intervals, and simplifying the notation by using (7) leads to:

$$\begin{aligned} K_P(V_1^2+V_2^2) - Q_{DC_P}NV_{DC} = \frac{Q_{DC_P}Q_{AV}}{C_{res}} \rightarrow K_P = \frac{Q_{DC_P}(NV_{DC}+\frac{Q_{AV}}{C_{res}})}{V_1^2+V_2^2}, \\ K_N(V_3^2+V_4^2) + Q_{DC_N}NV_{DC} = \frac{Q_{DC_N}Q_{AV}}{C_{res}} \rightarrow K_N = \frac{Q_{DC_N}(-NV_{DC}+\frac{Q_{AV}}{C_{res}})}{V_3^2+V_4^2}. \end{aligned} \tag{11}$$

As the transient operation should ideally converge to the steady-state operation, the steady-state value for Q_{AV} as shown in (9) will be used to calculate K_P and K_N in (11). For the two cases addressed before, the charge levels at which switching actions and commutations need to start and end can be derived, as shown in Table I. Similar to steady-state operation, after the active phases, the neutral line is conducting until the charge reaches its final value. Note that in both cases the intervals corresponding to V_4 and V_1 are always skipped for $I_{res} > 0$ and $I_{res} < 0$, respectively. Initial and final charge levels are expected to be the same in steady-state. In an implementation, the value of Q_{initP} can be obtained by sampling the value of the voltage across C_{res} at the zero crossing of I_{res} while the values for $Q_{endP} = Q_{initN}$ and Q_{endN} are calculated using ($Q_{initN} = Q_{AV} + 0.5Q_{DC}$) and ($Q_{endN} = Q_{AV} - 0.5Q_{DC}$).

Charge level #	Case 1 (12Z4)	Case 2 (1Z34)
$Q_{comm}(1)$	Q_{initP}	Q_{initP}
$Q_{comm}(2)$	$Q_{comm}(1)+K_PV_1$	$Q_{comm}(1)+K_PV_1$
$Q_{comm}(3)$	$Q_{comm}(2)+K_PV_2$	Q_{endP} (skip V_3)
$Q_{comm}(4)$	Q_{endP} (skip V_4)	Q_{endP} (skip V_4)
$Q_{comm}(5)$	Q_{initN}	Q_{initN}
$Q_{comm}(6)$	$Q_{comm}(5)+K_NV_4$	$Q_{comm}(5)+K_NV_4$
$Q_{comm}(7)$	Q_{endN} (skip V_2)	$Q_{comm}(6)+K_NV_3$
$Q_{comm}(8)$	Q_{endN} (skip V_1)	Q_{endN} (skip V_1)

Table I: Charge levels for switching actions per case.

Simulation tests

To verify the intended operation of the circuit and its control, a simulation model was built using the PLECs blockset [12] in the Simulink environment [13]. In Figure 4, results for steady state operation when supplying a 48V load with 1 kW are shown where the input line voltage is 400 V_{AC}, 50 Hz. The transformer ratio is selected as 4 to provide an easy operating range for the 400 V_{AC} input voltage of the converter.

The natural resonant frequency is set to 5000 Hz. This very low resonant frequency value is used to increase visibility in the figures, in practice a much higher frequency can be used. The red waveforms are representing the averaged value of the current (blue) waveforms and as shown in Figure 4b the averaged phase current looks sinusoidal. The averaged phase current in Figure 4b and phase voltage in Figure 4a are in the same phase which indicates that, after removal of the HV part by a low-pass filter, unity power factor is successfully achieved. The average of neutral line current, I_Z, is zero in the Figure 4c as expected.

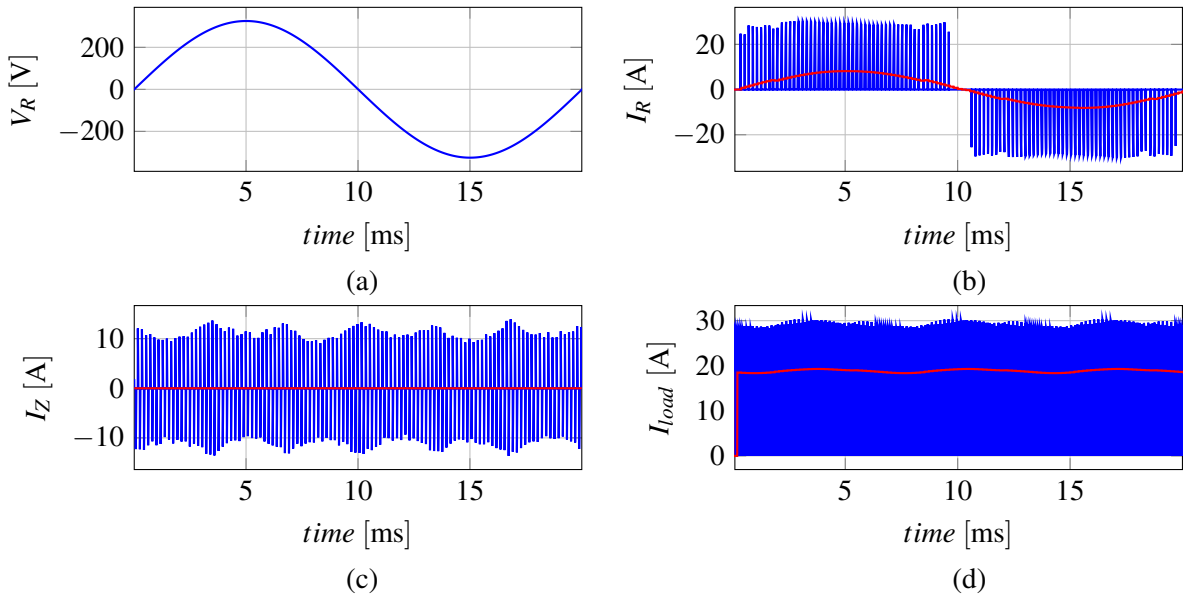

Fig. 4: Simulation results: (a) phase R voltage (b) phase R current and its average (c) zero line current and its average (d) load current and its average.

A more detailed spectral analysis is presented in Figure 5 for the normalized phase R current. The fundamental 50 Hz component is shown as first order in the Figure 5. The calculated total harmonic distortion using simulation results is 2.21%. Compared to the fundamental component, other components are quite insignificant. The results are similar for the other phases.

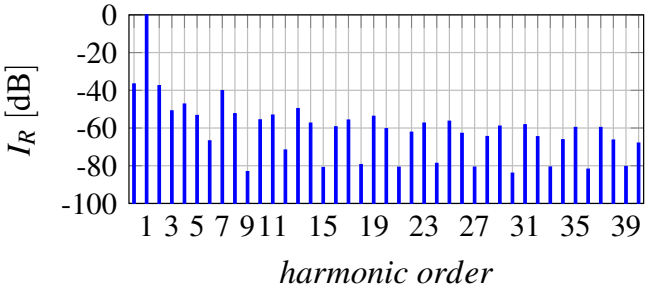

Fig. 5: Spectral analysis of the phase R current for the first 40 harmonic components.

Conclusion

Analytic derivations and simulation results are presented for the proposed novel control method which is applied to a fully zero-voltage switching series-resonant isolated 3-phase AC to DC converter. The simulation results show that the proposed control method is a promising approach to operate a fully zero-voltage switching series-resonant isolated 3-phase AC to DC converter, achieving unity power factor and low total harmonic distortion.

References

[1] J. Choi, D. Tsukiyama and J. Rivas, "Evaluation of a 900 V SiC MOSFET in a 13.56 MHz 2 kW resonant inverter for wireless power transfer," 2016 IEEE 17th Workshop on Control and Modeling for Power Electronics (COMPEL), 2016, pp. 1-6.

[2] H. Kim, A. Anurag, S. Acharya and S. Bhattacharya, "Analytical Study of SiC MOSFET Based Inverter Output dv/dt Mitigation and Loss Comparison With a Passive dv/dt Filter for High Frequency Motor Drive Applications," in IEEE Access, vol. 9, pp. 15228-15238, 2021.

[3] J. L. Schanen, A. Baraston, M. Delhommais, P. Zanchetta, and D. Boroyevitch, "Sizing of power electronics emc filters using design by optimization methodology," 2016 7th Power Electronics and Drive Systems Technologies Conference (PEDSTC), pp. 279–284, 2016.

[4] H. Huisman, I. de Visser and J. Duarte, "Optimal trajectory control of a CLCC resonant power converter," 2015 17th European Conference on Power Electronics and Applications (EPE'15 ECCE-Europe), 2015, pp. 1-10, doi: 10.1109/EPE.2015.7309101.

[5] R. Bonten, J. M. Schellekens, B. Vermulst, F. Clermonts and H. Huisman, "Improved Dynamic Behaviour for the Series-Resonant Converter using Bidirectional Charge Control," in IEEE Transactions on Power Electronics, doi: 10.1109/TPEL.2022.3169710.

[6] R. W. T. Bonten, J. M. Schellekens, H. Huisman and C. G. E. Wijnands, "A Comparative Evaluation of Series-Resonant, Bidirectional Optimal Trajectory Controlled Isolated DC-DC Converters," 2019 21st European Conference on Power Electronics and Applications (EPE '19 ECCE Europe), 2019, pp. P.1-P.10, doi: 10.23919/EPE.2019.8915383.

[7] G. E. Sfakianakis, J. Everts, H. Huisman, T. Borrias, C. G. E. Wijnands and E. A. Lomonova, "Charge-based ZVS modulation of a 3–5 level bidirectional dual active bridge DC-DC converter," 2016 IEEE Energy Conversion Congress and Exposition (ECCE), 2016, pp. 1-10, doi: 10.1109/ECCE.2016.7854914.

[8] R. W. T. Bonten, J. M. Schellekens and H. Huisman, "Optimal Utilization of the Dual-Active Bridge Converter with Bidirectional Charge Control," 2021 22nd IEEE International Conference on Industrial Technology (ICIT), 2021, pp. 452-457, doi: 10.1109/ICIT46573.2021.9453656.

[9] H. Huisman, "A three-phase to three-phase series-resonant power converter with optimal input current waveforms. I. Control strategy," in IEEE Transactions on Industrial Electronics, vol. 35, no. 2, pp. 263-268, May 1988, doi: 10.1109/41.192658.

[10] F. P. Kusumah and J. Kyyra, "Successive injections modulation of a direct three-phase to single-phase ac/ac converter for a contactless electric vehicle charger," The Journal of Engineering, vol. 2019, no. 17, pp. 4106–4110, 2019.

[11] R. Oruganti, Fred C. Lee, "Resonant Power Processors, Part I State Plane Analysis", IEEE Trans. On Industry Applications, vol. IA-21, No. 6, Nov./Dec. 1985, pp. 1453-1460.

[12] Plexim engineering software documentation, Plecs blockset packages, 2002. [Online]. Available: https://www.plexim.com/documentation.

[13] Simulink documentation, Simulation and model-based design, 2020. [Online]. Available: https://www.mathworks.com/products/simulink.html.